267. Finite Element Analysis of Thermo-Elastical Modal Damping of MEMS Vibrations

R. Barauskas[1], S. Kausinis[2], Ingrid De Wolf[3], S. Stoffels[4], H. A. C. Tilmans[5]
[1]Kaunas University of Technology, Studentu 50-407, LT-51368, Kaunas, Lithuania, **E-mail:** *rimantas.barauskas@ktu.lt*
[2]Kaunas University of Technology, K. Donelaicio 73, LT-44029, Kaunas, Lithuania, **E-mail:** *saulius.kausinis@ktu.lt*
[3]Interuniversity Microelectronics Center, Kapeldreef 75, B-3001, Leuven, Belgium, **E-mail:** *Ingrid.DeWolf@imec.be*
[4]Interuniversity Microelectronics Center, Kapeldreef 75, B-3001, Leuven, Belgium, **E-mail:** *stoffels@imec.be*
[5]Interuniversity Microelectronics Center, Kapeldreef 75, B-3001, Leuven, Belgium**, E-mail:** *Harrie.Tilmans@imec.be*

Abstract

The paper deals with finite element analysis of damped modal vibrations Q-factor values determined by thermal-elastic damping in micro-electrical-mechanical systems (MEMS). Mathematically the problem is formulated as a complex eigenvalue problem. Verification problems have been solved by using several computational environments and different presentations of model equations in order to comprehend and reduce the influence of rounding errors. The analysis of damped modal properties of selected real MEMS resonator revealed the main features of thermal-elastic damping by taking into account 3D geometry of the resonator and anchoring (clamping) structure.

Keywords: thermal-elastic damping, finite element modeling, MEMS, resonator

1. Introduction

Physical models of vibration damping in structures are complex. Mathematical models of traditional machines and mechanisms often included correct terms describing damping (friction) forces in kinematic pairs and enabled to obtain corresponding solutions. Performances of dampers could be measured experimentally and thereafter used for indicating precisely their mechanical effect upon the structure. In practical calculations very often the damping forces were evaluated approximately, however, the main reason for making simplifications was the desire to obtain simpler expressions and easier solved equations. For example, if only linear velocity proportional damping is assumed, complex eigenvalues λ of the structure can be calculated by applying well-known numerical algorithms. The imaginary parts of eigenvalues identify the eigenfrequencies of the structure, and the ratio of imaginary and real parts as $Q = \left| \dfrac{\text{Im}(\lambda)}{2 * \text{Re}(\lambda)} \right|$ evaluate the quality factor (*Q*-factor, dynamic amplification factor) of the vibrating structure. This kind of information in many cases can be regarded as sufficient for the characterization of main dynamic properties of the structure. The reasoning for the selection of damping coefficient value is that the computed and experimental results should agree. This value should be treated as a certain generalized characteristic of a specific structure, which integrally takes into account numerous effects and conditions of internal and external friction.

Smaller linear dimensions of new systems and structures implicate different constructions and compositions. Traditional kinematic pairs and linkages between links of the structures are abandoned and the functionality ensured by employing controlled deformation or vibration of elastic parts. The damping effect takes place mostly due to internal friction forces created in the material. Correct mathematical description of such damping forces is more complex, as in most cases the forces cannot be measured directly. In structures with linear dimensions of millimeters or centimeters approximate linear damping models are often applied. Basing on the assumption that the losses in vibrating piezoelectric structures is conditioned by mechanical, piezoelectric and electric phenomena, linear damping terms are used in the dynamic equations. Though the nature of real damping forces is quite complicated, approximately it is presented by the hysteretic loop of the stress-strain relationship. If harmonic vibration is analyzed, the hysteretic is approximately described by introducing complex-valued stiffness coefficients as $[\mathbf{c}] = [\overline{\mathbf{c}}](1 + j\eta_M)$, where η_M is the *mechanical dissipation factor*. Its physical meaning is the phase angle between stresses and strains of the harmonically vibrating structure. The complex value of $[\mathbf{c}]$ implies that the calculations are performed in frequency domain, therefore the stiffness matrix of the structure is presented in complex form as $[\mathbf{K}](1 + j\eta_M)$. Mathematically the same effect could be obtained by using the linear damping term $[\mathbf{C}]\{\dot{\mathbf{U}}\}$ in the finite element structural equation, where $[\mathbf{C}] = \eta_M[\mathbf{K}]$ is the proportional damping matrix, $[\mathbf{K}]$ - stiffness matrix, $\{\mathbf{U}\}$ - nodal displacement vector. The general form of the proportional damping matrix reads as $[\mathbf{C}^e] = a_1[\mathbf{M}^e] + a_2[\mathbf{K}^e]$, where coefficients a_1, a_2 are

21

easily found by virtue of known values of the Q-factor of the structure corresponding to two modal frequencies. Very similar consideration could lead to complex values of electromechanical and dielectric permittivity coefficients, [1]. Such simplified vibration damping models are applicable where the damping is not high and where the aim of calculation is to investigate the dynamic behavior of a structure at given values of its Q-factor.

Investigating electromechanical systems in micro- and nano-electrical-mechanical system (MEMS and NEMS) range of dimensions poses even more complex problems of adequate evaluation of structural damping. Though usually the continuum-based finite element models are applied for presenting strains and stresses, the proportional damping assumptions appear as too rough and imprecise. The Q-factors of MEMS often are very high and may reach $10^5 - 10^9$. The new MEMS designs require to predict the expected value of Q-factor of the system and to know, which particular factors may influence this value. In reference [2] a comprehensive analysis of physical phenomena influencing the vibration damping in GaAs and Si mono-crystal resonators has been performed. The influence of temperature, magnetic fields, frequency and linear dimensions of MEMS has been investigated experimentally. Physical causes of damping can be identified as thermal-elasticity, clamping losses, coupled anharmonic modes, surface anisotropy and internal defects. In the measured cases the friction at the zones of internal defects has been recognized as the main reason of damping. In [3] experimental investigations of MEMS-gyro have been directed to the analysis of thermal-elastic damping. The electronic circuit damping ($Q \approx 3.5 \times 10^{11}$), thermal-elastic damping ($Q = 3.3 \times 10^4$ - 8.29×10^5) and damping caused by other factors ($Q \approx 2.5 \times 10^5$) have been distinguished. On the base of the obtained results the conclusion could be drawn that for a particular MEMS-gyro structure thermal-elastic damping appears as a very important factor determining the overall Q-factor of the vibrations. Clamping losses appeared to have the main influence among of the damping sources caused by other factors.

Certain theoretical investigations in the field of thermal-elastic damping have been performed as early as in ~1930-40, [4]. The formula for obtaining the Q-factor of the first bending mode of a clamped beam has been derived, [5]. The analytical investigation of the first longitudinal mode of an unsupported beam has been performed in [6], and analytical results have been compared against the finite element modeling results. Satisfactory coincidence of results has been obtained under an assumption that the temperature values at ends of the beam are known and constant. In reality, the assumption of prescribed beam end temperatures lacks a sound physical explanation, however, the temperature values at this zone may be assumed to vary within a very small range due to negligibly small strains at the ends of an

unsupported beam. Finite element software COMSOL Multiphysics has been employed for calculations in [6], where the „coefficient" form of the presentation of equations has been chosen. However, no analysis could be found regarding the possible loss of numerical accuracy during the solution of the eigenproblem, which may be significant as the real parts of the eigenvalues in practical cases are up to $10^5 - 10^9$ times smaller than the imaginary ones.

This work presents the finite element analysis of eigenfrequencies and Q factors of sample structures and real MEMS structures by taking into account thermal-elastic effects and the influence of the geometry of the clamping zone.

2. Finite element model

MEMS are etched 3D structures, which consist of the active Si structure separated from the foundation substrate by the SiO_2 intermediate layer. The vibrations of active elements are excited by means of interaction forces among electric charges supplied to appropriate zones of the structure. Even in case of linear models of physical phenomena, the deformation of MEMS under the action of electrical field is described by non-linear equations. During deformation processes of active elements the 3D MEMS geometry, as well as, electrical field strength are not constant.

The eigenvalue problem of MEMS vibrations at the first approximation may be assumed as linear. The reasoning for such assumption is that the modal analysis is performed without taking into account the excitation forces, which are the main cause of the non-linearity of the electro-mechanical coupling. The model presented in this work is presented as a system of partial differential equations (PDE), which describe the elastic and thermal phenomena in the MEMS structure.

Elastic vibrations of solids are described in volume V and its surface S by means of PDE as

$$\left[\mathbf{A}\right]^T \left\{\boldsymbol{\sigma}\right\} + \left\{\mathbf{b}\right\} = \rho \left\{\ddot{\mathbf{u}}\right\}, \qquad \in V \qquad (1)$$

and boundary conditions as:

$$\left\{\mathbf{t}\right\} = \left[\mathbf{A}_s\right]^T \left\{\boldsymbol{\sigma}\right\}, \qquad \in S \qquad (2)$$

where $\left\{\boldsymbol{\sigma}\right\}$ - stress tensor in Foigt's notation, $\left\{\mathbf{b}\right\}$ - body force vector, $\left\{\mathbf{t}\right\}$ - surface force vector, given on surface S, $\left\{\mathbf{u}\right\}$ - displacement vector of any point of the volume, ρ - mass density, $\left[\mathbf{A}\right]$ - differential operator, $\left[\mathbf{A}_s\right]$ - matrix containing the components of the external normal vector $\left\{\mathbf{n}\right\}$ of surface S. In a general 3D case we have

$$[\mathbf{A}] = \begin{bmatrix} \frac{\partial}{\partial x} & 0 & 0 & 0 & \frac{\partial}{\partial z} & \frac{\partial}{\partial y} \\ 0 & \frac{\partial}{\partial y} & 0 & \frac{\partial}{\partial z} & 0 & \frac{\partial}{\partial x} \\ 0 & 0 & \frac{\partial}{\partial z} & \frac{\partial}{\partial y} & \frac{\partial}{\partial x} & 0 \end{bmatrix}^T \quad ; \quad [\mathbf{A}_s] = \begin{bmatrix} n_x & 0 & 0 & 0 & n_z & n_y \\ 0 & n_y & 0 & n_z & 0 & n_x \\ 0 & 0 & n_z & n_y & n_x & 0 \end{bmatrix} \quad .$$

The constitutive equation relates stresses, strains and temperature as

$$\{\boldsymbol{\sigma}\} = [\mathbf{c}]\left(\{\boldsymbol{\varepsilon}\} - [\kappa](T - T_0)\right) \tag{3}$$

where $\{\boldsymbol{\varepsilon}\}$ - strain tensor in Foigt's notation; $[\mathbf{c}]$ - stiffness tensor, $\{\boldsymbol{\kappa}\} = \{\kappa \quad \kappa \quad \kappa \quad 0 \quad 0 \quad 0\}^T$ - vector of thermal expansion coefficients, T - temperature at any point of the body, T_0 - reference temperature (i.e., the absolute temperature of a body is $T_0 + T$).

The temperature of the body is not known in advance as physical laws of thermodynamics govern them. The generation of heat due to elastic strain rate should be treated as one of body sources of heat. The heat exchange is described by the diffusion PDI as

$$\lambda_x \frac{\partial^2 T}{\partial x^2} + \lambda_y \frac{\partial^2 T}{\partial y^2} + \lambda_z \frac{\partial^2 T}{\partial z^2} + b_T - T_0[\kappa]^T[\mathbf{c}]\{\dot{\boldsymbol{\varepsilon}}\} = c_v \dot{T}, \in V \tag{4}$$

where:

T - temperature [K];
b - body source of heat; positive if the heat is supplied to the body, [W/m^3];
q - heat flux density; positive if the heat is withdrawn from the body [W/m^2];
α - coefficient of heat convection between the body and the surrounding [$W/(Km^2)$];
λ - heat conduction coefficient, [$W/(Km)$];
$c_v = \rho c_p$ - volumetric heat capacity of the material [$J/(m3 \ K)$];

c_p - mass heat capacity of the material [$J/(K \ kg \ )$]; ρ - density of the material [$kg/\ m^3$]; The boundary conditions on surface S are presented as

$$\lambda_x \frac{\partial T}{\partial x} n_x + \lambda_y \frac{\partial T}{\partial y} n_y + \lambda_z \frac{\partial T}{\partial z} n_z + \alpha(T - T_\infty) = 0, \quad \in S_\alpha$$

$$\lambda_x \frac{\partial T}{\partial x} n_x + \lambda_y \frac{\partial T}{\partial y} n_y + \lambda_z \frac{\partial T}{\partial z} n_z + q = 0, \quad \in S_q ,$$

$$T = T_p, \quad \in S_p , \tag{5}$$

(5) represent three possible types of boundary conditions. On surface S_p the temperature values are prescribed. On surfaces S_α and S_q the heat flux density normal to the surface is defined as $-\lambda_x \frac{\partial T}{\partial x} n_x - \lambda_y \frac{\partial T}{\partial y} n_y - \lambda_z \frac{\partial T}{\partial z} n_z$, however, the two equations define its value in two different ways. On surface S_α the value of heat flux density is proportional to the difference of temperatures of the body and of the surrounding one. Thermally isolated surfaces are defined by assuming $\alpha = 0$. On surface S_q the heat flux density is considered as being prescribed and equal to q, which is positive when the heat is withdrawn from the body.

By applying weighted residual techniques, from PDE (1) and (4), boundary conditions (2) and (5) and constitutive equation (3) we derive the matrix equation of a finite element as:

$$\begin{bmatrix} [\mathbf{M}] & 0 \\ 0 & 0 \end{bmatrix}\begin{Bmatrix} \{\ddot{\mathbf{U}}\} \\ 0 \end{Bmatrix} + \begin{bmatrix} [\mathbf{C}] & 0 \\ T_0[\mathbf{H}]^T & T_0[\tilde{\mathbf{C}}_T] + [\mathbf{C}_T] \end{bmatrix}\begin{Bmatrix} \{\dot{\mathbf{U}}\} \\ \{\dot{\mathbf{T}}\} \end{Bmatrix} + \begin{bmatrix} [\mathbf{K}] & -[\mathbf{H}] \\ 0 & [\mathbf{K}_T] \end{bmatrix}\begin{Bmatrix} \{\mathbf{U}\} \\ \{\mathbf{T}\} \end{Bmatrix} = \begin{Bmatrix} \{\mathbf{R}\} + \{\mathbf{P}\} - [\mathbf{H}]\{\mathbf{T}_0\} \\ \{\mathbf{P}_T\} + \{\mathbf{S}_T\} + \{\mathbf{S}_\infty\} + \{\mathbf{Q}\} + [\mathbf{K}_T]\{\mathbf{T}_0\} \end{Bmatrix} \tag{6}$$

Where $[\mathbf{M}] = \int_V \rho[\mathbf{N}]^T[\mathbf{N}]dV$, $[\mathbf{K}] = \int_V [\mathbf{B}]^T[\mathbf{c}][\mathbf{B}]dV$ - mass and stiffness matrices;

$[\mathbf{B}] = [\mathbf{A}][\mathbf{N}]$;

$[\mathbf{N}]$ and $[\mathbf{N}_T]$ - form function matrices, which interpolate displacements and temperatures within a finite element;

$[\mathbf{C}] = a_1[\mathbf{M}] + a_2[\mathbf{K}]$ - proportional damping matrix, where a_1, a_2 - coefficients.

$[\mathbf{C}_T] = c_v \int_V [\mathbf{N}_T]^T[\mathbf{N}_T]dV$ - heat capacity matrix of the element; $[\mathbf{K}_T] = \int_V [\mathbf{B}_T]^T[\mathbf{\Lambda}][\mathbf{B}_T]dV + \alpha \int_V [\mathbf{N}_T]^T[\mathbf{N}_T]dS$ - heat conduction matrix of the element;

$$[\mathbf{B}_T] = grad\left([\mathbf{N}_T]\right) = \begin{bmatrix} \frac{\partial}{\partial x} \\ \frac{\partial}{\partial y} \\ \frac{\partial}{\partial z} \end{bmatrix}[\mathbf{N}_T];$$

23

$[\mathbf{\Lambda}] = [diag(\lambda)]$ - heat conduction coefficients;

$[\mathbf{H}] = \int_V [\mathbf{B}]^T [\mathbf{c}][\kappa][\mathbf{N}_T] dV$ - thermal-elastic matrix of the element;

$\{\mathbf{P}\} = \int_V [\mathbf{N}]^T \{\mathbf{b}\} dV$ - nodal force vector determined by body forces;

$\{\mathbf{P}_T\} = \int_V [\mathbf{N}_T]^T b_T dV$ - nodal power vector, determined by prescribed body heat sources; $\{\mathbf{S}_T\} = -\int_{S_q} [\mathbf{N}_T]^T q dS$ - nodal power vector, determined by prescribed heat flux

density across the surface; $\{\mathbf{S}_\infty\} = \alpha T_\infty \int_{S_\alpha} [\mathbf{N}_T]^T dS$ - nodal power vector, determined by thermal exchange with the surrounding across the surface;

$\{\mathbf{Q}\}$ - vector of prescribed nodal power;

$\{\mathbf{R}\}$ - vector of prescribed nodal forces.

During the investigation of modal vibration the right-hand side vector in (6) is assumed as zero. Second order differential equation system (6) can be transformed to the first order differential equation system by performing substitution $\{\mathbf{V}\} = \{\dot{\mathbf{U}}\}$. The obtained first order differential equation system reads as

$$\begin{bmatrix} [\mathbf{M}] & 0 & 0 \\ 0 & [\mathbf{I}] & 0 \\ 0 & 0 & T_0[\tilde{\mathbf{C}}_T]+[\mathbf{C}_T] \end{bmatrix} \begin{Bmatrix} \{\dot{\mathbf{V}}\} \\ \{\dot{\mathbf{U}}\} \\ \{\dot{\mathbf{T}}\} \end{Bmatrix} + \begin{bmatrix} [\mathbf{C}] & [\mathbf{K}] & -[\mathbf{H}] \\ -[\mathbf{I}] & 0 & 0 \\ T_0[\mathbf{H}]^T & 0 & [\mathbf{K}_T] \end{bmatrix} \begin{Bmatrix} \{\mathbf{V}\} \\ \{\mathbf{U}\} \\ \{\mathbf{T}\} \end{Bmatrix} = \begin{Bmatrix} 0 \\ 0 \\ 0 \end{Bmatrix} \quad , \quad (7)$$

The eigenvalue problem is formlated as

$$\det \left(\begin{bmatrix} [\mathbf{C}] & [\mathbf{K}] & -[\mathbf{H}] \\ -[\mathbf{I}] & 0 & 0 \\ T_0[\mathbf{H}]^T & 0 & [\mathbf{K}_T] \end{bmatrix} + \lambda \begin{bmatrix} [\mathbf{M}] & 0 & 0 \\ 0 & [\mathbf{I}] & 0 \\ 0 & 0 & T_0[\tilde{\mathbf{C}}_T]+[\mathbf{C}_T] \end{bmatrix} \right) = 0 \quad . \quad (8)$$

After eigenvalue (8) is solved, the obtained complex eigenvalues define the Q-factor of the structure as

$$Q = \left| \frac{\text{Im}(\lambda)}{2 * \text{Re}(\lambda)} \right| \quad .$$

3 Analysis of results

3.1 Investigation of longitudinal vibration modes of a beam resonator

Investigation of longitudinal vibration modes of a beam resonator has been performed in order to verify the finite element model. The natural frequencies obtained by using different software and in different spatial dimensions (1D and 3D) of the same beam have been compared against each other. The material constants of the beam are as presented in Table 1, [6].

1D model in MATLAB environment has been implemented by using equations (6)-(8). In 1D case the uniaxial stress is assumed, however, strains are exhibited in all 3 spatial directions. In the case of isotropic material

their values are obtained from equation (3) presented in expanded form as (9):

Table 1

Si material constants

Material constant	Value	Units
Young's modulus, E	1.69e11	Pa
Mass density, ρ	2330	kg/(m^3)
Poison's coefficient, ϑ	0.3	-
Thermal expansion coefficient, κ	2.59 e-6	1/K
Mass specific heat , c_p	713	m^2/(K*s^2)
Thermal conduction coefficient, λ	156	kg*m/(K*s^3)
Reference temperature, T_{init}	290	K

24

$$\begin{Bmatrix} \sigma_x \\ \sigma_y \\ \sigma_z \\ \tau_{xy} \\ \tau_{yz} \\ \tau_{xz} \end{Bmatrix} = \frac{E(1-\vartheta)}{(1+\upsilon)(1-2\vartheta)} \begin{bmatrix} 1 & \frac{\vartheta}{1-\vartheta} & \frac{\vartheta}{1-\vartheta} & 0 & 0 & 0 \\ \frac{\vartheta}{1-\vartheta} & 1 & \frac{\vartheta}{1-\vartheta} & 0 & 0 & 0 \\ \frac{\vartheta}{1-\vartheta} & \frac{\upsilon}{1-\upsilon} & 1 & 0 & 0 & 0 \\ 0 & 0 & 0 & \frac{1-2\vartheta}{2(1-\vartheta)} & 0 & 0 \\ 0 & 0 & 0 & 0 & \frac{1-2\vartheta}{2(1-\vartheta)} & 0 \\ 0 & 0 & 0 & 0 & 0 & \frac{1-2\vartheta}{2(1-\vartheta)} \end{bmatrix} \begin{Bmatrix} \varepsilon_x - \kappa(T-T_0) \\ \varepsilon_y - \kappa(T-T_0) \\ \varepsilon_z - \kappa(T-T_0) \\ \gamma_{xy} \\ \gamma_{yz} \\ \gamma_{xz} \end{Bmatrix} \quad (9)$$

After substituting values $\sigma_z = \sigma_y = 0$ into (9) we obtain $\varepsilon_y = \varepsilon_z = -\vartheta\varepsilon_x + \kappa(\vartheta+1)(T-T_0)$.

Matrices of linear 2-node element are presented as

$$[\mathbf{C}_T] = c_v \int_V [\mathbf{N}_T]^T [\mathbf{N}_T] dV = \frac{c_v Al}{2}\begin{bmatrix} 1 & 0 \\ 0 & 1 \end{bmatrix}; \quad [\mathbf{K}_T] = \int_V [\mathbf{B}_T]^T [\mathbf{\Lambda}][\mathbf{B}_T] dV = \frac{\lambda A}{l}\begin{bmatrix} 1 & -1 \\ -1 & 1 \end{bmatrix};$$

$$[\mathbf{H}] = \int_V [\mathbf{B}]^T [\mathbf{c}][\kappa][\mathbf{N}_T] dV = \frac{AE\kappa}{2}\begin{bmatrix} -1 & -1 \\ 1 & 1 \end{bmatrix}; \quad [\tilde{\mathbf{C}}_T] = \frac{AlE\kappa^2(\vartheta+1)}{(1-2\vartheta)}\begin{bmatrix} 1 & 0 \\ 0 & 1 \end{bmatrix}. \quad (10)$$

After structural matrices are assembled, eigenvalue problem (8) is solved by using the MATLAB function `eig`. The results regarding the 1st longitudinal mode are presented in Table 2, 6th column. It appears important to mention the danger of possible loss of arithmetic accuracy of the solution. In case of linear measures corresponding to MEMS, numerical values residing in matrices of equation (8) may be of a very different magnitude. As a consequence, the eigenproblem solution process may diverge, or its accuracy may be lost. This regards mainly the real parts of eigenvalues, which may be up to $10^5 - 10^9$ times smaller than the imaginary ones. Proper scaling should be applied in order to avoid or diminish the above-mentioned effect. As one of the possible ways of scaling a proper change of units system may be applied.

Instead of basic units of SI as $[m,\ kg,\ s,\ K]$ we used the unit system $\left[\dfrac{m}{number\ of\ elements},\ kg,\ 10^{-7}s,\ 10^6 K\right]$.

1D model in COMSOL Script environment is presented in a "general" form

$$d_a \begin{Bmatrix} \dot{v} \\ \dot{u} \\ \dot{T} \end{Bmatrix} + \nabla \cdot \Gamma = F \qquad,\text{ which in 1D case reads as}$$

$$\begin{bmatrix} 0 & 1 & 0 \\ \rho & 0 & 0 \\ 0 & 0 & C_v + \frac{2T_0 c\kappa^2(\vartheta+1)}{1-2\vartheta} \end{bmatrix}\begin{Bmatrix} \dot{v} \\ \dot{u} \\ \dot{T} \end{Bmatrix} - \begin{bmatrix}\frac{\partial}{\partial x}\end{bmatrix}\begin{Bmatrix} 0 \\ c\frac{\partial u}{\partial x} - c\kappa T \\ \lambda\frac{\partial T}{\partial x} \end{Bmatrix} = \begin{Bmatrix} v \\ 0 \\ T_0 c\kappa v \end{Bmatrix}; \qquad \in V \quad, \quad (11)$$

where

$$d_a = \begin{bmatrix} 0 & 1 & 0 \\ \rho & 0 & 0 \\ 0 & 0 & C_v + \frac{2T_0 c\kappa^2(\vartheta+1)}{1-2\vartheta} \end{bmatrix}; \quad \Gamma = -\begin{Bmatrix} 0 \\ c\frac{\partial u}{\partial x} - c\kappa T \\ \lambda\frac{\partial T}{\partial x} \end{Bmatrix}; \quad F = \begin{Bmatrix} v \\ 0 \\ T_0 c\kappa v \end{Bmatrix}.$$

25

Boundary conditions are presented as

$$\begin{cases} -\vec{\mathbf{n}} \cdot \Gamma = G + \left(\dfrac{\partial R}{\partial u}\right)^{T} \mu; \quad \in S \\ 0 = R \qquad\qquad\qquad \in S \end{cases} \qquad (12)$$

where $G = \begin{bmatrix} 0 \\ 0 \\ 0 \end{bmatrix}, \quad R = \begin{bmatrix} 0 \\ 0 \\ T - T_0 \end{bmatrix}.$

The later boundary condition means that temperatures of certain points of a structure are known in advance (Dirichlet boundary condition). If the beam is thermally insulated the boundary conditions G and R are both zeros, i.e. the natural boundary conditions are valid by default.

As all equations are linear, the COMSOL "coefficient" form is applicable as

$$\begin{bmatrix} 0 & 1 & 0 \\ \rho & 0 & 0 \\ 0 & 0 & C_v + \dfrac{2T_0 c\kappa^2 (\vartheta+1)}{1-2\vartheta} \end{bmatrix} \begin{Bmatrix} \dot{v} \\ \dot{u} \\ \dot{T} \end{Bmatrix} - \dfrac{\partial}{\partial x} \begin{bmatrix} 0 & 0 & 0 \\ 0 & c & 0 \\ 0 & 0 & \lambda \end{bmatrix} \dfrac{\partial}{\partial x} \begin{Bmatrix} v \\ u \\ T \end{Bmatrix} - \dfrac{\partial}{\partial x} \begin{bmatrix} 0 & 0 & 0 \\ 0 & 0 & -\kappa c \\ 0 & 0 & 0 \end{bmatrix} \begin{Bmatrix} v \\ u \\ T \end{Bmatrix} + \begin{bmatrix} 0 & 0 & 0 \\ 0 & 0 & 0 \\ T_0 \kappa c & 0 & 0 \end{bmatrix} \dfrac{\partial}{\partial x} \begin{Bmatrix} v \\ u \\ T \end{Bmatrix} + \begin{bmatrix} -1 & 0 & 0 \\ 0 & 0 & 0 \\ 0 & 0 & 0 \end{bmatrix} \begin{Bmatrix} v \\ u \\ T \end{Bmatrix} = 0$$

The results regarding the 1st longitudinal mode are presented in Table 2, 5th column.

3D model in COMSOL Multiphysics environment has been created by using the GUI as a coupled two-field Multiphysics problem. Two application modes have been coupled:

• MEMS Module-> Structural Mechanics->Plane Stress->Damped eigenfrequency analysis;
• COMSOL Multiphysics->Heat Transfer ->Conduction->Transient analysis.

Thermal-mechanical coupling is ensured by entering the body heat source, which described the generation of the heat in the volume at given strain rates as $-\dfrac{T_0 \kappa c}{1-2\vartheta}\left(\dfrac{\partial \dot{u}}{\partial x} + \dfrac{\partial \dot{v}}{\partial y} + \dfrac{\partial \dot{w}}{\partial z}\right)$ and the expansion of the solid due to temperature variation $T - T_0$. The results regarding the 1st longitudinal mode are presented in Table 2, 5th column

Analysis of the results of Table 2 demonstrates that TED phenomena cause only very slight increase (~0.01%) of the modal frequency compared with the modal frequency obtained without considering TED, 2nd and 3rd columns of Table 2. However, the most important result of the calculation is the obtained Q-factor value (note that without considering TED the theoretical value of the Q-factor should be infinite as no internal friction effects are considered in the model). For verification purposes Table 2 presents the Q-factor values obtained for 1D and 3D models.

4 column of Table 2 presents the results obtained in [6], and 5th and 6th columns display the results obtained in this work by using the MATLAB and COMSOL Script models described above. It is worth to mention that columns 4-6 present the results of analysis of mathematically identical (!) models, however, slightly different results (up to 1-2%) can be observed. It seems reasonable to assume that different numerical values are caused by rounding errors, which are caused by specific values of coefficients of PDEs. Though the accuracy of calculations is satisfactory for engineering purposes, the calculations should be performed very carefully and additional effort should be devoted in order to persuade that the solution is within acceptable accuracy limits. Proper selection of physical unit system, as well as, scaling of variables may facilitate to obtain good solutions. Comparing the solutions obtained by using different scaling coefficients against each other also facilitate the understanding if the rounding errors do not influence the solution significantly. Results also may appear as slightly different, depending on eigenvalue problem solution algorithm used.

Increased attention should be also devoted to the investigation of convergence of the solution. It is well known that in the solution of purely mechanical modal analysis problem only few elements are enough for obtaining the first mode of a structure. Even a single element is able to approximate reasonably the first modal frequency. If thermal-elastic damping is taken into account the number of elements should be much greater. For example, a single element is completely unable to represent the effect of TED, as its first eigenvalue is obtained as entirely complex (i.e. it does not describe the damping effect). The solutions in examples above have been obtained by using 70 first order or 35 second order elements along the length of the beam.

Fig.1 presents the eigenform of distribution of amplitude values of temperature along the beam during its 1st mode longitudinal vibration. The temperature values should be interpreted as relative ones rather than defined in Kelvin as they are determined by modal forms, which are dimensionless. Therefore relative values of temperature are presented by the contour plot over a domain. They change harmonically all the time as the resonator vibrates. The TED effect on modal vibrations depends on the reference

26

temperature T_0, i.e. on temperature of the structure before the experiment. The value of the modal frequency increases only very slightly with the increase of

temperature, however, the Q-factor value is much more sensitive to the reference temperature variation, Fig. 2.

Table 2

Modal frequencies and Q-factors of 1st longitudinal mode of unsupported MEMS beams. Thermal-elastic damping (TED) taken into account at the condition of full thermal insulation

Length (μm)	1st modal frequency (Hz)		Q-factor			
	Without TED	With TED	Ref. [6]	1D, COMSOL Script, 35 II order elements	1D model, MATLAB, 70 I order elements	3D model, COMSOL Multiphysics
0.5	8.51587e+009	8.51667e+009	1.0004e+005	1.002715e+005	1.0065e+005	1.005578e5
5	8.51587e+008	8.51671e+008	7.8963e+005	7.91674e+005	7.98966e+005	7.938552e5
50	8.51587e+007	8.51671e+007	7.4744e+006	7.48993e+006	7.66816e+006	7.513373e6
500	8.51587e+006	8.51671e+006	7.3515e+007	7.32553e+007	7.64718e+007	7.375455e7
1000	4.25793e+006	4.25835e+006	1.4670e+008	1.46297e+008	1.52940e+008	1.470492e8
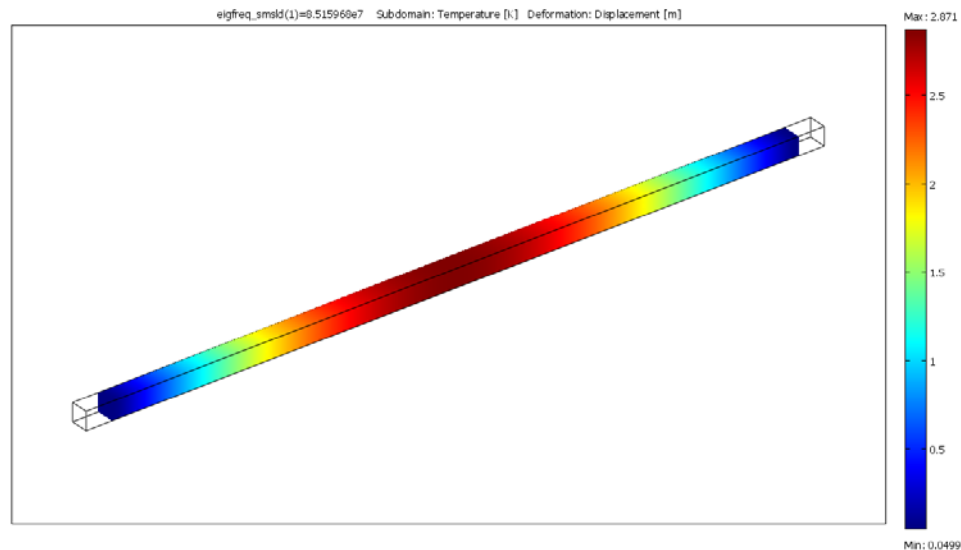
Fig. 1. Distribution of amplitude values of temperature along an unsupported beam resonator at 1st longitudinal mode
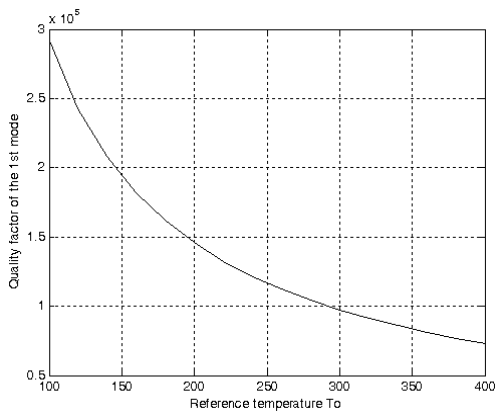

Fig. 2. Dependance of the Q-factor of the first longitudinal mode of an unsupported beam resonator against the reference temperature

3. 2 Investigation of bending vibration modes of a beam resonator

A 3D computational model of bending vibrations of a beam resonator in COMSOL Multiphysics environment is very similar to the one used in section 3.1 for longitudinal vibration analysis. The only difference is that the bending vibration model employs a single symmetry plane *xOz* along the beam, while two symmetry planes *xOz* and *xOy* have been used for longitudinal vibration investigation. The finite element mesh and 1 and 3 modal vibration forms are presented in Fig.3, where contours depict the temperature distribution over the beam caused by the thermal-elastic coupling. The beam is assumed to be completely thermally isolated.

27
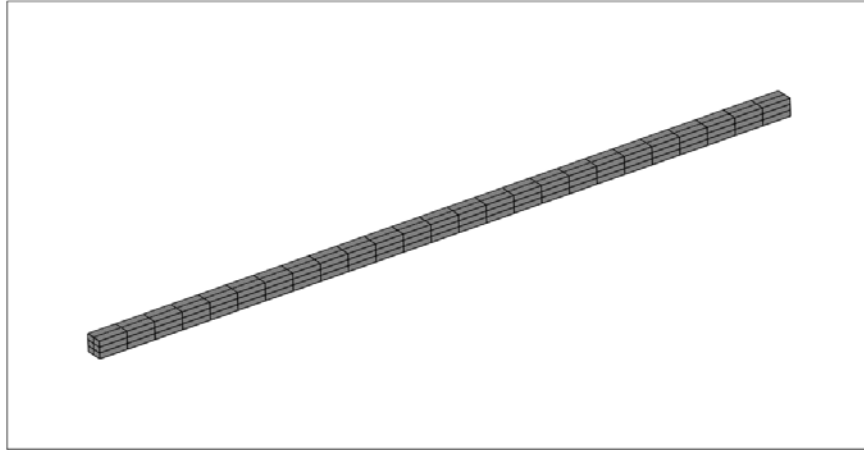
(a)
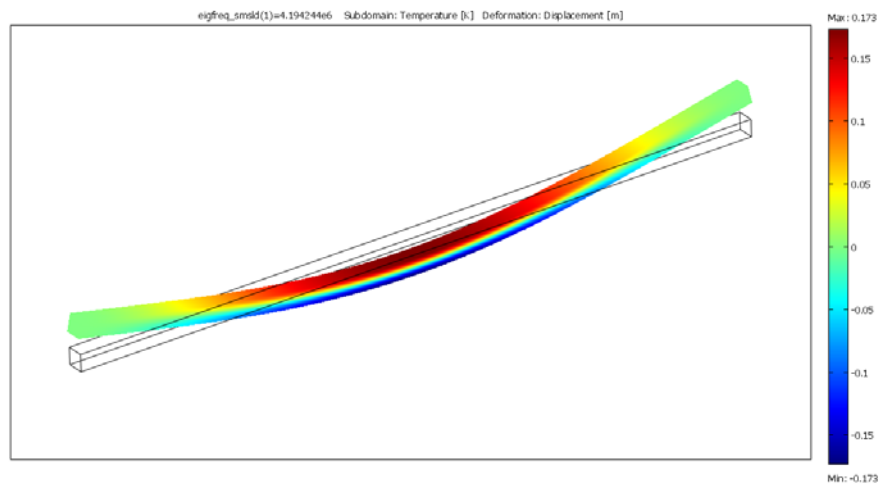
(b)
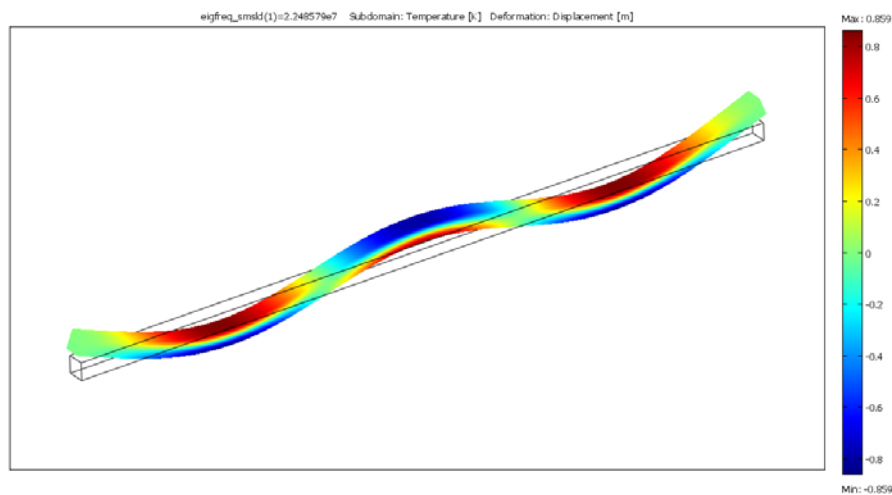
(c)

Fig. 3. Distribution of amplitude values of temperature at modal bending vibration of an unsupported beam resonator; length of the beam L=50 µm, cross-section height h=1.2 µm;
a) finite element mesh, symmetrical model; b) 1st mode, f = 4194244 Hz; Q = 125715.6;

28

Fig. 4 depicts the 1st modal form of the same beam resonator clamped at both ends. The temperatures at the ends of the beam are assumed as known and equal to reference temperature T_0. The assumption is based on the fact that the clamped ends of the beam comprise a monolithic body with other parts and the base (substrate) of the body of MEMS chip.
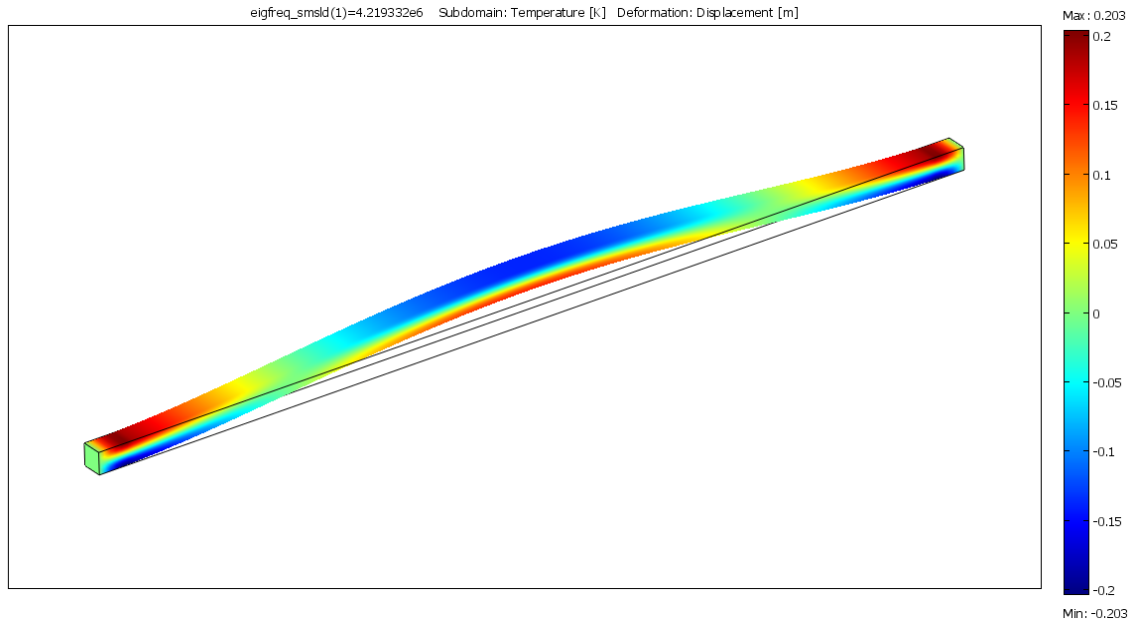

Fig. 4. Distribution of amplitude values of temperature at modal bending vibration of a beam resonator ideally clamped at the ends; f = 4219332 Hz; Q = 130337

The influence of thermal boundary conditions and of the reference temperature on the Q-factor of the 1st bending mode may be analyzed, Table 3. If the temperatures at the ends of the beam are considered as given, the Q-factor of the bending mode is always calculated as larger than it would be for fully thermally isolated beam. The effect of thermal isolation of the beam was quite opposite when longitudinal vibrations were considered, [6].

Table 3

1st modal frequency and Q factor of a beam clamped at its ends at different reference temperature values

	Ends of the beam thermally isolated		Temperature of ends of the beam equal to reference temperature	
T_0 (K)	f (Hz)	Q	f (Hz)	Q
100	4219332	320665	4219332	377978
200	4219332	160332	4219332	188989
290	4219332	110574	4219332	130337
400	4219332	80167	4219332	94495

3.3 Investigation of bending modes of resonators structures in 3D

A layout of a sample resonator depicted in Fig. 5a presents an etched 3D structure, which consists of the active Si structure including the beam-type resonator and anchor, which is separated from the foundation substrate by the SiO_2 intermediate layer. The anchors are resting on the intermediate layer meanwhile the intermediate layer material under the beam part of the resonator is removed.

The resonator is able to perform in-plane and out-of-plane bending vibrations. The finite element models corresponding to positive and negative clamping (anchoring) angles are depicted in Fig. 5 b, c. The models present only active layer and intermediate layer the bottom surface of which was approximately assumed to be supported fixedly. Symmetric out of plane modes can be calculated by using a quarter symmetry model as in Fig. 6 b, c and symmetric in-plane modes can be presented by using a symmetrical model as in Fig.7. The values of

29

material constants of SiO$_2$ used in our calculations are presented in Table 4

<div align="right">**Table 4**</div>

<div align="center">SiO$_2$ material constants</div>

Material constant	Value	Units
Young's modulus, E	0.73e11	Pa
Mass density, ρ	2200	kg/(m^3)
Poison's coefficient, ϑ	0.17	-
Thermal expansion coefficient, κ	0.55e-6	1/K
Mass specific heat , c_p	1000	m^2/(K*s^2)
Thermal conduction coefficient, λ	1.4	kg*m/(K*s^3)
Reference temperature, T_{init}	290	K

The results obtained in case of ideally clamped beam (columns 6-7 of Table 5) produce a ~10% error both in modal frequency and the Q-factor. Therefore the ideally clamped beam model can be applied only for very rough estimations of the dynamic behavior of real resonators. The analysis results substantiate the necessity to employ 3D models, which represent full geometry of anchors and the intermediate layer. However, clamping geometry can be expected to be neither the reason nor the explanation of "clamping losses" mentioned elsewhere in the literature as the Q-factors of models containing the full clamping geometry produce Q-factor values even higher than those of ideally clamped beam model. Probably, the internal friction properties of SiO$_2$ material should be investigated in order to provide the theoretical background for the clamping losses effect. The influence of reference temperature on the Q-factor value may be analyzed from Table 5, where the increase of reference temperature causes the rapid decrease of the Q-factor value.

Numerical results of the 1st out-of-plane bending vibration mode in Table 6 present the values of modal frequency and Q-factors at two different clamping angles $+30^o$, -30° and in case of ideally clamped ends of the resonator, the distribution of amplitude values of temperature over the structure corresponding to the 1st mode being presented in Fig.7. The dependence of the Q-factor values on the reference temperature exhibits the same tendency as it was in the case of out-of-plane vibrations. The necessity of using 3D models presenting full 3D clamping geometry is obvious because of large difference in modal frequencies presented in columns 2 and 4 against column 6.

<div align="right">**Table 5**</div>

<div align="center">Frequencies and Q-factors of the 1st out-of-plane bending mode of MEMS resonator at different values of the reference(surrounding) temperature and different anchoring conditions</div>

T$_0$ (K)	Clamping angle +30°		Clamping angle -30°		Ideal console clamping	
	f (Hz)	Q	f (Hz)	Q	f (Hz)	Q
100	7547432	122478	7731439	115290	8256405	108662
200	7547437	61240	7731475	57646	8256409	54331
290	7547443	42236	7731481	39756	8256413	37470
400	7547449	30621	7731488	28824	8256419	27166

<div align="right">**Table 6**</div>

<div align="center">Frequencies and Q-factors of the 1st in-plane bending mode of MEMS resonator at different values of the reference(surrounding) temperature and different anchoring conditions</div>

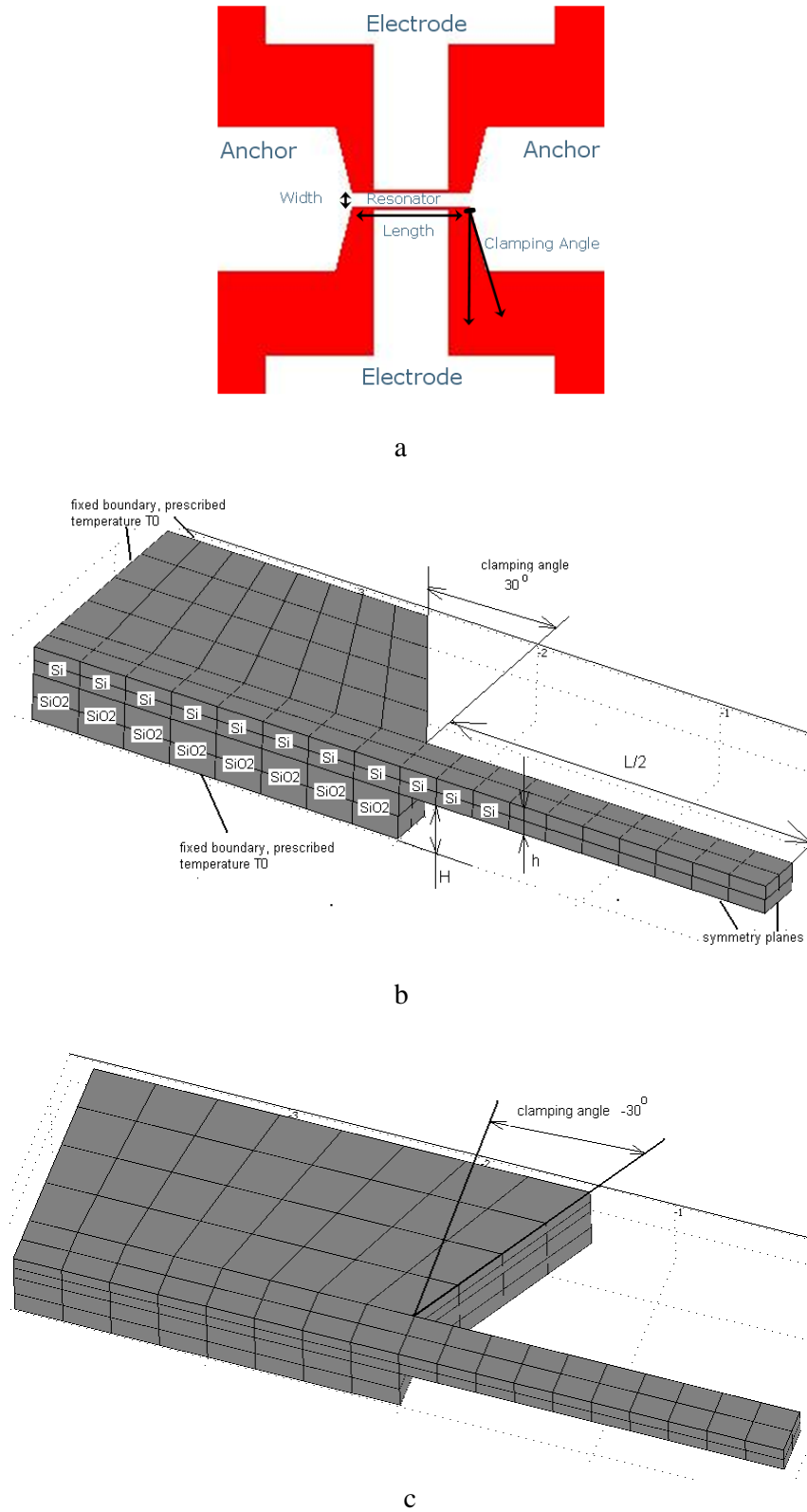| T$_0$ (K)	Clamping angle +30°		Clamping angle -30°		Ideal console clamping	
	f (Hz)	Q	f (Hz)	Q	f (Hz)	Q
100	22 049 920	61950	22 459 710	58778	25 074 130	59512
200	22 050 500	31000	22 460 290	29412	25 074 800	29780
290	22 051 020	21395	22 460 810	20298	25 075 400	20553
400	22 051 650	15525	22 461 450	14729	25 076 130	14914

30

a

b

c

Fig. 5. Principal scheme of MEMS structure(a) and quarter-symmetry models for calculating the „out of plane" bending modes at positive (b)and negative (c) values of the clamping angle; length of the beam L, cross-section height h, width of the beam b, height(thickness) of SiO_2 layer H
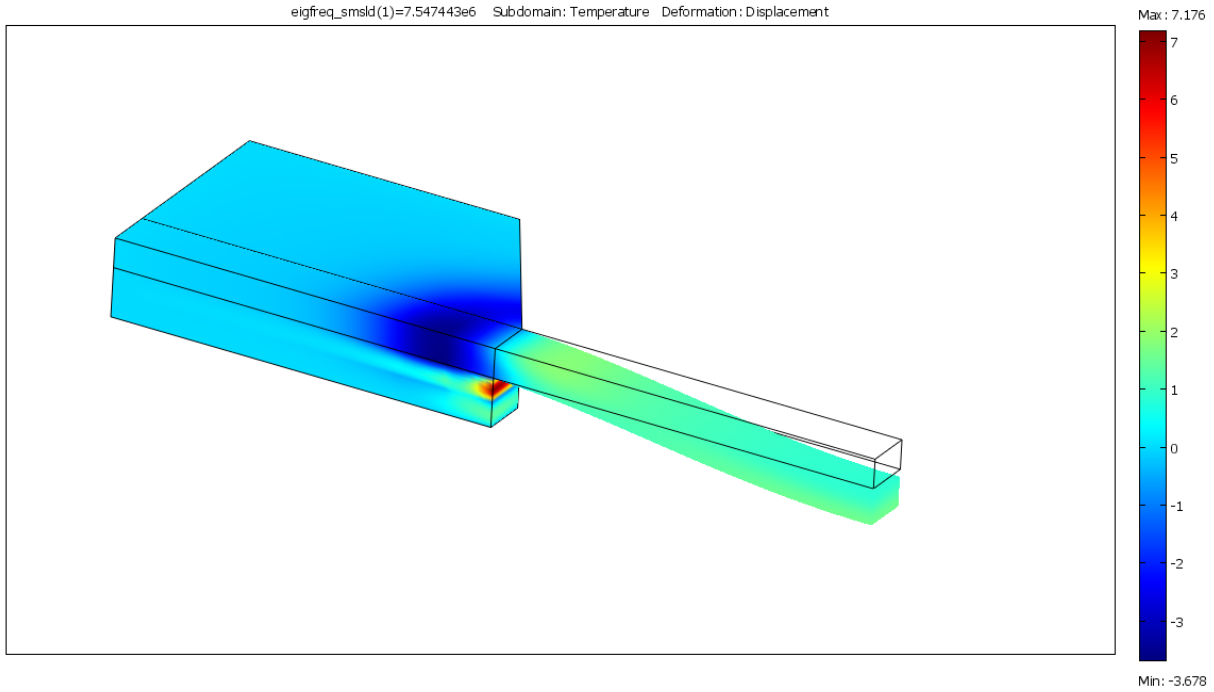
31

Fig. 6. Distribution of amplitude values of temperature at 1st out-of-plane bending mode vibration of a beam clamped at its ends; length of the beam L = 40 µm, height of the cross-section h=1.5 µm, width of the beam b = 5 µm, height (thickness) of SiO$_2$ layer H = 2.5 µm, clamping angle +30°; quarter-symmetry model, f = 7547443 Hz; Q = 42236
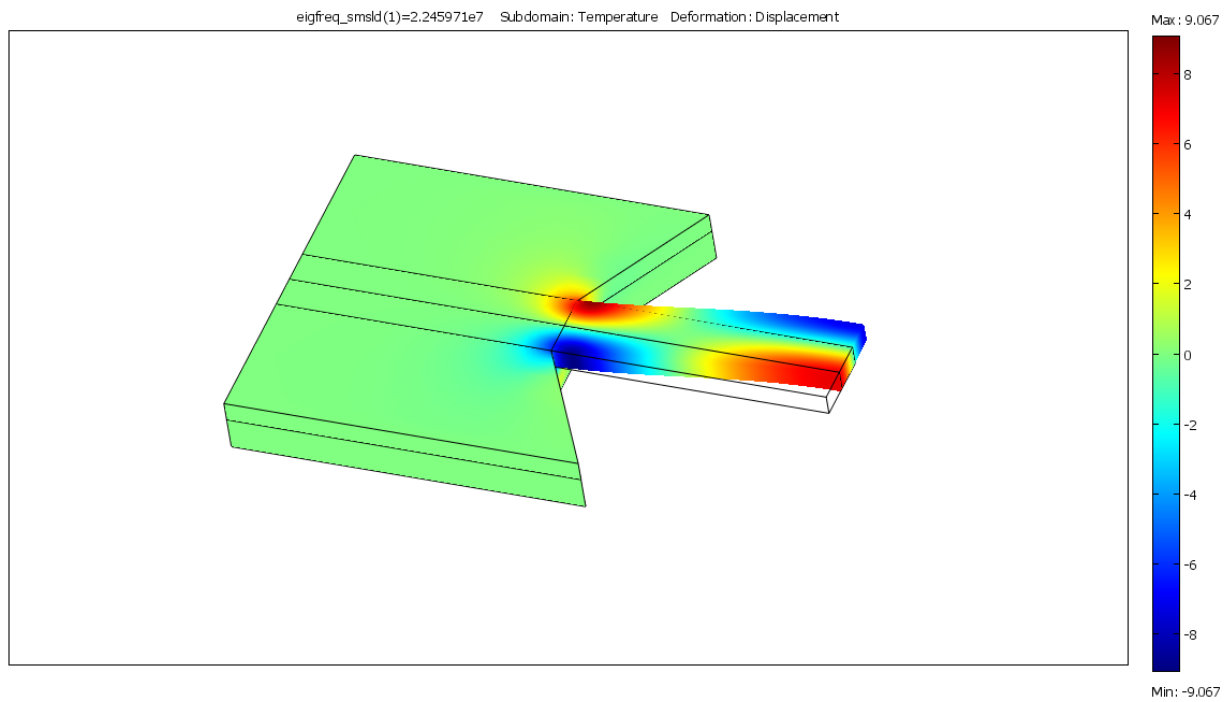

Fig. 7. Distribution of amplitude values of temperature at 1st in-plane bending mode vibration of a beam clamped at its ends; length of the beam L = 40 µm, height of the cross-section h = 1.5 µm, width of the beam b = 5 µm, height (thickness) of SiO$_2$ layer H = 2.5 µm, clamping angle -30°; symmetric model, f = 22 460 810 Hz; Q = 20298

32

4. Conclusions

The Q-factor determined by thermal-elastic damping of micro-electro-mechanical resonators structures is a very important dynamic characteristic since it provides the upper limit of the Q-factor that is possible to achieve in a structure of given geometry and materials under an assumption that no internal friction and other sources of damping are present.

A FEM computational model of longitudinal and bending vibrations of a beam resonator has been developed in order to analyze the eigenfrequencies and Q factors of test vehicle as well as real MEMS structures. Model verification has been performed by calculating modal properties of unsupported beam structures and comparing against published results.

The analysis of the micro-electro-mechanical resonator revealed the main features of thermal-elastic damping by taking into account 3D geometry of the resonator and the anchoring (clamping) structure. The clamping angles and reference temperature have a significant influence on modal frequencies and Q-factors of the resonator. However, the calculations performed could not explain the clamping losses effect mentioned in the reference literature and suggests further investigations in this direction where the internal damping in silicon dioxide intermediate layer of the MEMS chip should be investigated in more details by setting-up properly planned physical and numerical experiments.

References

1. **Barauskas R.** Analysis and synthesis of elastic structures with unilateral constraints. Computer methods and application to the controlled vibrational systems, Kaunas, Technologija, 1992.-299psl.,
2. **Mohanty P., Harrington D. A., Ekinci K. L., Yang Y. T., Murphy M. J., and Roukes M. L.** Intrinsic dissipation in high-frequency micromechanical resonators, PHYSICAL REVIEW B 66, 085416 ~2002!
3. **Amy E. Duwel, John P. Gorman, Marcie Weinstein, Jeffrey T., Borenstein, Paul A. Ward**, Quality Factors of MEMS Gyros and the Role of Thermoelastic Damping, © IEEE. Reprinted with permission from the Proceedings of the 15th IEEE International Conference on Microelectromechanical Systems (MEMS), Las Vegas, NV, January 20-25, 2002, pp. 214 -219.
4. **Clarence Zener**, *Physical Review.V52-53,(1937-1938)*
5. **Nowick A. S. and Berry B. S.** *Anelastic Relaxation in Crystalline Solids, Academic Press 1972*.
6. **Weibin Zhang , Kimberly L. Turner**, Thermoelastic damping in longitudinal vibration: anglysis and simulation, Proceedings of IMECE04, 2004 ASME International Mechanical Engineering Congress and Exposition November 13-20, 2004, Anaheim, California USA, IMECE2004-59898.
7. **Zienkiewitcz O.** The *Finite Element Method,vol.1:The Basis,* Butterworth Heinemann, 2000, 689p.

33